ChemCatChem

ChemCatChem
Chemistry Europe
European Chemical Societies Publishing

RESEARCH ARTICLE OPEN ACCESS

Improved Copper-Zinc Based Catalysts for the Partial Dehydrogenation of Dicyclohexylmethanol

Lukas Maurer[1,2] | Lucas Warmuth[3] | Maximilian Thiele[1,2] | David Guse[4] | Matthias Kind[4] | Peter Wasserscheid[1,2,5] | Stephan Pitter[3] | Moritz Wolf[3,6] | Franziska Auer[1]

[1]Helmholtz-Institute Erlangen-Nürnberg for Renewable Energy (IET-2), Forschungszentrum Jülich GmbH, Erlangen, Germany | [2]Institute of Chemical Reaction Engineering (CRT), Friedrich-Alexander-Universität Erlangen-Nürnberg (FAU), Erlangen, Germany | [3]Institute of Catalysis Research and Technology (IKFT), Karlsruhe Institute of Technology (KIT), Eggenstein-Leopoldshafen, Germany | [4]Institute for Thermal Process Engineering (TVT), Karlsruhe Institute of Technology (KIT), Karlsruhe, Germany | [5]Institute for a Sustainable Hydrogen Economy (INW), Forschungszentrum Jülich Gmbh, Jülich, Germany | [6]Engler-Bunte-Institut, Karlsruhe Institute of Technology (KIT), Karlsruhe, Germany

Correspondence: Franziska Auer (f.auer@fz-juelich.de)

Received: 6 November 2025 | **Revised:** 23 December 2025 | **Accepted:** 13 January 2026

Keywords: alcohol | aurichalcite | catalyst synthesis | dehydrogenation | hydrogen

ABSTRACT

$Cu/ZnO/ZrO_2$ (CZZ) catalysts outperform conventional $Cu/ZnO/Al_2O_3$ (CZA) materials in methanol synthesis. Building on recent findings that CZA catalysts enable hydrogen release from the oxygen-containing LOHC compound dicyclohexylmethanol (H14-BP) below 200°C, this study investigates structure-activity correlations with CZZ catalysts in the partial dehydrogenation of H14-BP as a model reaction. CZZ materials were produced by continuous co-precipitation with subsequent batch suspension ageing. A ZrO_2 content between 4 and 8 mol% increased the specific surface area and catalytic activity. Zn-rich materials with elevated aurichalcite $[(Cu,Zn)_5(OH)_6(CO_3)_2]$ content in the catalyst precursor achieved higher activity despite a reduced specific surface area. Ageing at 70°C promoted aurichalcite formation and improved performance, whereas higher temperatures reduced the specific surface area. An initial pH value of 6.7 enhanced Zn uptake during ageing and increased dehydrogenation productivity by 45% compared to pH 7.1. High catalyst productivity correlated with aurichalcite contents up to 98% and small crystallite sizes. Overall, CZZ outperformed CZA catalysts in the partial dehydrogenation of H14-BP, with the aurichalcite phase playing a crucial role. Our results demonstrate the potential of this material class for selective dehydrogenation reactions and enable targeted further development based on the correlation between material-specific properties and catalytic activity.

1 | Introduction

Transporting and storing renewable energy is vital for the global energy transition. In this regard liquid organic hydrogen carriers (LOHCs) are a highly promising option for hydrogen storage and transport, serving as an energy vector compatible with existing infrastructure [1]. Technically relevant LOHC systems include aromatic hydrocarbons and their hydrogenated counterparts, such as toluene/methylcyclohexane [2, 3], (perhydro) dibenzyltoluene (H18-/H0-DBT) [4–7], and (perhydro) benzyltoluene (H12-/H0-BT) [4, 7]. The covalent binding of hydrogen significantly enhances the volumetric energy density.

Binding and release of hydrogen to/from LOHC molecules is realized via catalytic reactions. The high enthalpy of the dehydrogenation reaction thereby prevents accidental hydrogen release

Lukas Maurer & Lucas Warmuth contributed equally to this work

under ambient conditions but also requires significant energy input to maintain the reaction temperature. Alternative LOHC systems and more efficient catalysts can reduce dehydrogenation temperatures, leveraging heat integration potentials. LOHC systems containing heteroatoms like nitrogen in (perhydro) *N*-ethylcarbazole (H12-/H0-NEC) have been extensively studied, enabling dehydrogenation temperatures below 200°C. Nitrogen-containing LOHC systems generally exhibit reduced hydrogenation/dehydrogenation enthalpies [8]. Researchers have recently investigated the suitability of oxygen-containing molecules as LOHCs. Zakgeym et al. [9] experimentally demonstrated that dicyclohexylmethanol (H14-BP) can be dehydrogenated at temperatures below 250°C, yielding benzophenone (H0-BP). The authors also showed that the alcohol functionality can be dehydrogenated using a Cu-based catalyst achieving a selectivity of 100%. Hence, the overall hydrogen capacity including reversibly bound hydrogen in the aromatic rings increases to 7.2 wt% when compared to 6.7 wt% for the oxygen-free counterpart, (perhydro) diphenylmethane (H12-/H0-DPM) [10]. Recently, a commercial $Cu/ZnO/Al_2O_3$ (CZA) catalyst was demonstrated to enable the dehydrogenation of the alcohol functionality at temperatures as low as 150°C [9].

CZA catalysts are also widely used for methanol synthesis on industrial scale [11–15]. In this regard $Cu/ZnO/ZrO_2$ (CZZ) catalysts show enhanced productivity and stability, especially for CO_2-rich feeds [16–22]. Cu/Zn aluminate catalysts are also suitable for ethanol dehydrogenation to acetaldehyde [23]. Interestingly, also in this reaction ZrO_2 showed a positive influence on the performance of Cu-based catalysts [24, 25]. Thus, in this study, we present a CZZ catalyst as an efficient alternative to CZA for hydrogen release from the alcohol functionality of the model LOHC compound H14-BP. The catalyst precursors are produced by continuous co-precipitation with subsequent batch suspension ageing. This allows for temporal and spatial separation of precipitation and ageing to enable fine-tuning of the catalyst properties (e.g. porosity, composition, crystal structure and others) which was demonstrated for methanol synthesis [26–28]. It is known for these systems that the initial synthesis generates structural motifs, which inherit the later application [29]. Thus, focused variation of precursor synthesis and the assessment of the resulting catalyst characteristics (e.g. crystal phases) is studied for the evaluation of catalyst performance on partial hydrogen release from H14-BP as a model reaction.

2 | Experimental section

2.1 | Catalyst Synthesis

The CZZ precatalyst was prepared by continuous co-precipitation with subsequent ageing. The details of the procedure are described elsewhere [26]. In short, a solution of copper(II) nitrate trihydrate ($Cu(NO_3)_2{\cdot}3\,H_2O$, Merck, Darmstadt, Germany, 99.5%), zinc nitrate hexahydrate ($Zn(NO_3)_2{\cdot}6\,H_2O$, Alfa Aesar, Thermo Fischer, Kandel, Germany, 99%) and zirconium(IV) oxynitrate hexahydrate ($ZrO(NO_3)_2{\cdot}6\,H_2O$, Sigma–Aldrich/Merck, Darmstadt, Germany, 99%) in 3 L of deionized water (metal salt contents for standard synthesis, see Table 1) is mixed under high volume flow with a solution of Na_2CO_3 at 55°C—as not stated otherwise—using a specific Y-shaped nozzle. The created suspension was transferred directly to a double-jacketed 5000 mL glass vessel and aged at elevated temperature under continuous stirring (1000 rpm) until reaching the characteristic pH-tipping point plus additional 30 min. Afterwards the aged suspension was filtered, and the filter cake was washed with distilled water until filtrate conductivity of <50 µS cm^{-1} was reached. The obtained greenish / turquoise solid was then dried and calcined at 350°C prior to use as described elsewhere [30].

The catalytic materials are labeled according to their composition as $Cu_xZn_yAl_z$(-com) or $Cu_xZn_yZr_z$(-T)(-pH) with x, y, z being the molar proportions of Cu, Zn and Al/Zr, respectively. "Com" thereby identifies the commercial reference material. "T" indicates the ageing temperature if different from the standard value of 55°C. A variation of the initial pH value in the ageing step differing from the standard of 7.1 is specified through an additional value in the material labeling if applicable.

2.2 | Catalyst Characterization

2.2.1 | Inductively coupled plasma optical emission spectroscopy (ICP-OES)

For determining the atomic composition (Cu, Zn, Zr and potential catalytic "poisons" such as halides, Na, Fe or Ni) of the CZZ catalyst, ICP-OES was applied. At first, a hydrofluoric acid digestion of 20 mg sample was carried out. Digestion was performed with an *Anton Paar Multiwave 3000* microwave oven using HF (40%) in Teflon vessels at 240°C for 2 h. Subsequent dilution was performed with 0.2 M HNO_3 Suprapur. For analysis, an *Agilent 725 ICP-OES* spectrometer with argon as plasma gas at 15 L min^{-1} and plasma stimulation at 40 MHz, 2 kW was used.

2.2.2 | X-ray diffraction (XRD)

X-ray diffractograms were measured using a Panalytical X'Pert Pro X-ray diffractometer (Malvern Panalytical GmbH, Kassel, Germany) with Bragg-Brentano geometry and Cu K_α radiation with a Ni filter. The diffractograms were recorded in the range 5–80° over a period of 120 min. The reflections were evaluated using the HighScore Plus software (version 2.2.5) and compared to references from the Joint Committee of Powder Diffraction Standards (JCPDS) database. To obtain the composition, particle size and Zn introduction of the samples analyzed by XRD, Rietveld refinement was performed using the open-source program Profex 5.0.2 [31]. The amount of Zn in the (zincian) malachite phase is determined by a linear fit regarding the work of Behrens et al. [32]. Here, a Vegard-type behavior is observed up to a Zn content of 31 mol%. [33]

2.2.3 | Nitrogen physisorption

N_2 physisorption measurements [34] were carried out on Quantachrome NOVA 2000e and NOVA 3200e devices (Anton Paar GmbH, Graz, Austria) at 77 K to determine the catalyst specific surface area. Samples (250 mg, grain size 250–500 µm) were degassed for 12 h at 230°C. Isotherms are evaluated with the Brunauer–Emmett–Teller (BET) model [35] in the range of 0.05–0.3 p/p_0.

TABLE 1 | Metal salt contents used in the synthesis of representative CZ catalyst materials, dissolved in deionized water.

Compound	Mass $Cu_{64}Zn_{32}Zr_4$ / g	Mass $Cu_{64}Zn_{27}Al_9$ / g	Mass $Cu_{67}Zn_{33}Zr_0$-70-8.0 / g
$Cu(NO_3)_2 \cdot 3\ H_2O$	117.42	117.42	58.71
$Zn(NO_3)_2 \cdot 6\ H_2O$	72.29	72.29	144.58
$ZrO(NO_3)_2 \cdot 6\ H_2O$	27.49	–	27.49
$Al(NO_3)_3 \cdot 9\ H_2O$	–	30.39	–
Na_2CO_3	256.32	323.38	120.12
Ageing temperature / °C	55	55	70

2.2.4 | Temperature-programmed reduction (TPR)

TPR was measured using an AutoChem III (version 1.02; Micromeritics). A 10% H_2 flow in Ar (45 mL min^{-1}) was used for the reduction. Samples were heated at 5 K min^{-1} up to 500°C. Data was analyzed and evaluated using MicroActive software (version 7.00; Micromeritics).

2.3 | Synthesis of H14-BP

H14-BP was produced by hydrogenation of benzophenone and had a purity of 98.42%.

2.4 | Dehydrogenation Experiments

The dehydrogenation experiments were carried out in a semi-batch glass setup as previously described [36, 37]. The experimental setup composed of a 100 mL three-neck glass flask with a reflux condenser and heating mantle. Temperature control of the liquid phase was achieved with a type K thermocouple inserted through a septum, combined with a Fitron 4 TP temperature controller, operated via FitronTP V1.0.2b software. To facilitate quantification of the hydrogen release, a continuous argon flow of 400 mL min^{-1} was maintained, which also shifts the reaction equilibrium toward dehydrogenation. This argon flow was precisely regulated using an EL-FLOW Prestige mass flow controller, monitored by Flow View V1.23 software. The off-gas, containing hydrogen and argon, passed through the reflux condenser and two washing bottles to eliminate organic residues. An activated carbon filter was employed to remove possible traces of other gaseous impurities. The hydrogen content in the gas stream was then measured using thermal conductivity (FTC 300; Messkonzept), calibrated for a range of 0–40 vol.% H_2 in Ar. The obtained volumetric flow of hydrogen was then used to calculate a catalyst productivity for each experiment according to Equations S1-S4 (see Supporting Information).

29.75 g (0.15 mol) of the hydrogen-loaded H14-BP was precisely weighed into the three-neck flask before starting the experiment. The catalyst amount was determined by a fixed molar ratio of LOHC to Cu of 100:1. The catalyst was placed in a custom-made stainless-steel sleeve inside a glass tube connected to the flask, allowing its release at the desired reaction temperature without exposing the system to air. The LOHC was magnetically stirred at 500 rpm and heated to the reaction temperature under argon flow. Once the LOHC reached the target temperature (170°C selected as standard from preliminary tests, see ESI), the catalyst was released. As soon as the evolution of the first hydrogen was measured, a 0.1 mL reference sample of the liquid phase was collected (0 min), defining the start of the experiment. Further 0.1 mL samples were taken at intervals of 5, 10, 20, 30, 40, 60, 90, and 120 min using a 1 mL plastic syringe and a cannula through the side-neck of the flask, which was sealed with a septum. These liquid samples were filtered to remove any residual catalyst particles and then prepared for gas chromatography (GC) analysis (Scheme 8).

The reaction scheme for the dehydrogenation of H14-BP is shown below, with the dehydrogenation of the alcohol functionality to H12-BP being the main reaction observed for Cu-based catalysts [9].

2.5 | Gas Chromatography of Liquid Samples

The liquid samples from the dehydrogenation experiments were analyzed using GC. A defined amount of the liquid sample was weighed into a GC vial, acetone was added as the solvent, and the mixture was homogenized by shaking. The samples were then analyzed with a Trace 1310 gas chromatograph (Thermo Fisher), equipped with an iConnect flame ionization detector (Thermo Fisher). Separation was achieved using a Rxi17Sil capillary column (Restek, 30 m, inner diameter 0.25 mm). A more detailed description of the procedure can be found in the ESI (Table S1), together with Equations S4–S7 used for all calculations.

3 | Results and Discussion

Initial tests were carried out with the standard temperature for the dehydrogenation experiments set to 170°C using the unground catalyst. Pepe et al. [38] investigated the dehydrogenation of isopropanol using $Cu/ZnO/Al_2O_3$ catalysts. The authors found that exclusively Cu is active for the dehydrogenation. Either way, two blank tests with ZnO and ZrO_2 were performed in the present study with no detectable conversion of H14-BP (Tables S2-S3).

As several catalyst compositions and precursor synthesis conditions were examined, an overview over the composition of all catalyst precursors and their phase composition as well as the specific surface area after calcination is shown in Table 2. Additionally, N_2 physisorption measurements reveal that the materials are mainly mesoporous with physisorption isotherms of IUPAC type IV. [34] Corresponding isotherms as well as

TABLE 2 | Summary of catalytic materials investigated: Molar composition, phase composition and specific surface area according to BET-method.

Catalytic material	Aurichalcite content $(Zn,Cu)_5[(OH)_6\|(CO_3)_2]$ / wt%	Malachite content $(CuZn_x)_2[(OH)_2\|CO_3]$ / wt%	A_{BET} / $m^2\ g^{-1}$
$Cu_{67}Zn_{32}Zr_0$	4	96	50
$Cu_{66}Zn_{33}Zr_1$	3	97	65
$Cu_{64}Zn_{32}Zr_4$	5	95	104
$Cu_{62}Zn_{30}Zr_8$	38	62	117
$Cu_{60}Zn_{30}Zr_{10}$	10	90	117
$Cu_{57}Zn_{27}Zr_{16}$-6.6	35	66	144
$Cu_{63}Zn_{27}Al_{10}$	–	–	102
$Cu_{66}Zn_{26}Al_7$-com	–	–	90
$Cu_{35}Zn_{61}Zr_4$	44	56	90
$Cu_{63}Zn_{32}Zr_5$-60	6	94	103
$Cu_{62}Zn_{32}Zr_6$-70	25	75	97
$Cu_{62}Zn_{31}Zr_7$-80	37	63	84
$Cu_{63}Zn_{30}Zr_7$-6.7	13	87	117
$Cu_{57}Zn_{27}Zr_{16}$	0	99	144
$Cu_{60}Zn_{30}Zr_{10}$-80-7.9	98	2	92
$Cu_{67}Zn_{33}Zr_0$-70-8.0	99	1	78

additional textural properties of representative catalytic materials are presented in the ESI (Figure S3, Table S4).

3.1 | Influence of Catalyst Composition

In the synthesis of methanol, the choice of promoter (most often Al_2O_3 or ZrO_2 for Cu/ZnO-based catalysts [39]) has a significant influence on the activity of the catalyst. By changing the promoter or its proportion, the structures of the metal oxides can be altered. This results in surface defects, which could form additional active centers. [40, 41] An increase of promotor amount above a critical proportion leads to the formation of secondary phases. The promoter accumulates in these phases and can form a Cu lean structure with ZnO [37, 38] leading to a decrease of the proportion of Zn in the malachite structure and with this, Cu dispersion also decreases. Inhomogeneous retaliation of the promoter in the precursor also leads to reduced defect formation.

ZnO is the mostly applied stabilizer for Cu-based methanol synthesis catalysts. According to Behrens et al. [42] Zn increases the adsorption strength of HCO, H_2CO and H_3CO while lowering the reaction barriers as it is incorporated into the Cu(211) surface. This results in better coverage of the catalyst surface under methanol synthesis conditions. Zn binds more strongly to these species and is partially oxidized, resulting in a stable intermediate oxidation state. According to Behrens [43], the highest dispersion of Cu should be achieved around a proportion of 50 mol% Zn.

To evaluate if similar effects come into account in the dehydrogenation of H14-BP, Cu/ZnO catalysts with 10 mol% Al_2O_3 ($Cu_{63}Zn_{27}Al_{10}$) and varying ZrO_2 contents between 0 and 16 mol% ($Cu_{67}Zn_{32}Zr_0$, $Cu_{66}Zn_{33}Zr_1$, $Cu_{64}Zn_{32}Zr_4$, $Cu_{62}Zn_{30}Zr_8$, $Cu_{60}Zn_{30}Zr_{10}$, $Cu_{57}Zn_{27}Zr_{16}$-6.6) as additives were prepared and compared to a catalyst without additive. In addition, a commercial Cu/ZnO/Al_2O_3 catalyst ($Cu_{66}Zn_{26}Al_7$-com, Alfa Aesar), which is currently the state of the art for the partial dehydrogenation of H14-BP [9], and one CZZ catalyst with an elevated Zn content of 61 mol% ($Cu_{35}Zn_{61}Zr_4$) according to the considerations above were analyzed. Particular changes in the material structure of the precatalysts are shown in Figure 1.

The use of ZrO_2 in CZZ instead of Al_2O_3 in CZA changes the surface area of the catalysts and therefore also the active surface

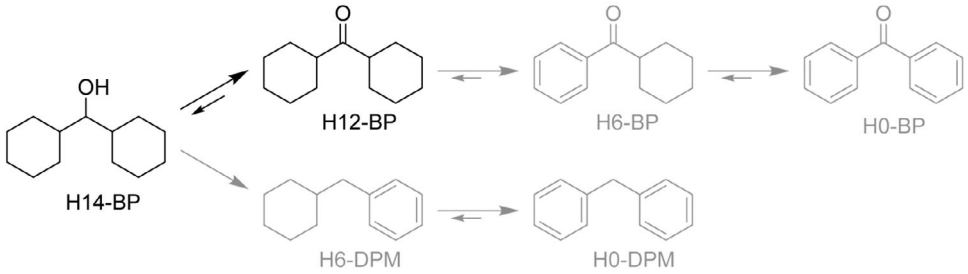

SCHEME 1 | Reaction scheme for the (partial) dehydrogenation of H14-BP, main reaction for Cu-based catalysts in black.

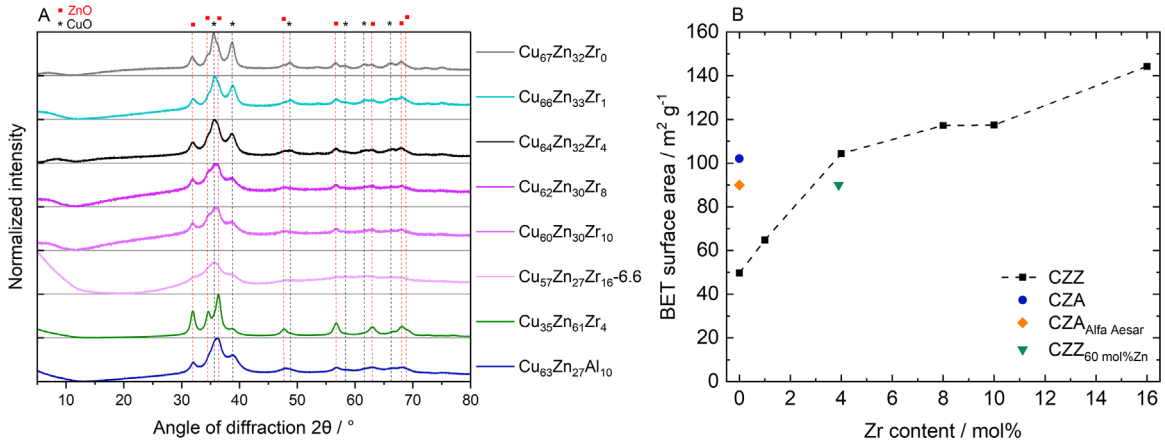

FIGURE 1 | (A) XRD measurements and (B) specific surface area according to the BET-method of the precatalysts with different compositions. Reference reflexes for ZnO (red square) and CuO (black star) included. Dashed line to guide the eye.

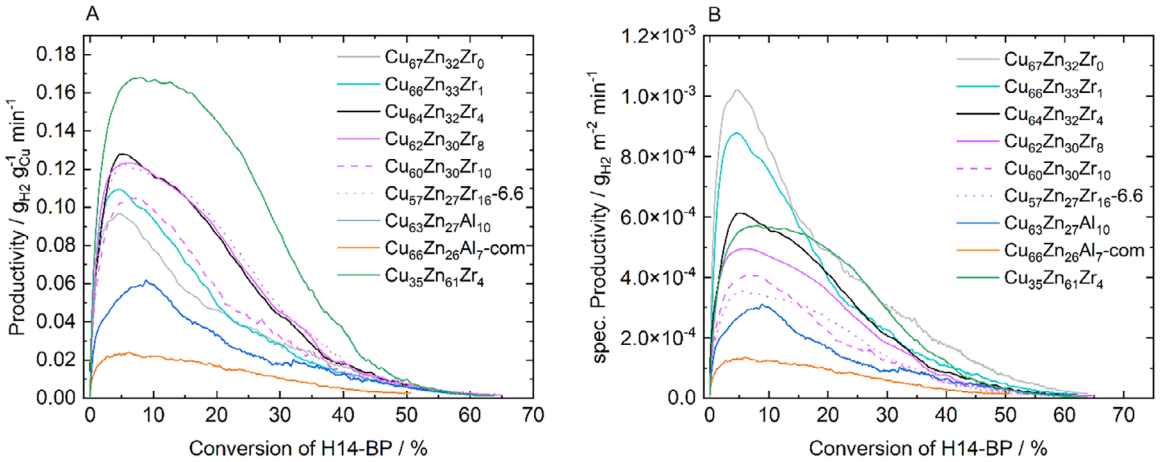

FIGURE 2 | Productivity (A) and specific productivity (B) over conversion of H14-BP of the catalysts with different zirconium content in the dehydrogenation of H14-BP. Experimental conditions: 170°C; 1 atm; 400 mL min^{-1} Ar; 1 mol% Cu:H14-BP; average from two dehydrogenation experiments.

area available for the reaction. The use of 10 mol% Al_2O_3 increases the specific surface area from 50 m^2 g^{-1} (for the catalyst without additive) to 102 m^2 g^{-1}. The use of the same amount of ZrO_2 leads to a further increase to 117 m^2 g^{-1}. Overall, a higher ZrO_2 content is associated with a higher specific surface area, as reported elsewhere [44, 45]. Moreover, XRD measurements reveal that reflexes are less defined for the materials with ZrO_2 than for the material without ZrO_2 indicating defects in the crystal lattice or a crystallites size decrease [46].

For the precursor with 61 mol% Zn, the specific surface area is lower than for the corresponding Cu-rich material. Synthetic malachite can contain up to 31 mol% Zn [33], homogeneously distributed in its needle-type morphology. Exceeding this value results in the formation of a Cu-lean and Zn-rich aurichalcite phase. However, platelets with a lower specific surface area are formed instead of a needlelike structure [43]. This increase of aurichalcite content is also observed in this study when comparing $Cu_{64}Zn_{32}Zr_4$ (5%) and $Cu_{35}Zn_{61}Zr_4$ (44%) (see Table 2).

The Cu-related productivity (Figure 2A) and surface normalized specific productivity (Figure 2B) of catalysts with different compositions in the partial dehydrogenation of H14-BP are compared in the following.

The tested catalysts show clear differences in their productivity at the beginning of the experiment whereas only minor differences can be observed at higher conversion, approaching the reaction equilibrium. In previous experiments, the reaction equilibrium at 170°C was determined at a H14-BP conversion of approx. 65%. All catalysts containing ZrO_2 show an increase in productivity (Figure 2A) when compared to the catalyst without additive ($Cu_{67}Zn_{32}Zr_0$). In contrast, modification by Al_2O_3 ($Cu_{63}Zn_{27}Al_{10}$) leads to a reduced productivity. The commercially available CZA catalyst ($Cu_{66}Zn_{26}Al_7$-com, Alfa Aesar) shows the lowest productivity.

Regarding Zr content, a volcano-type behavior can be identified considering the catalyst Cu-based productivity (see also Figure S4). Both the catalysts with 1 mol% and 10 mol% Zr, exhibit comparable productivity and slightly higher initial activity than the catalyst without Zr. The catalyst with 4 mol% Zr shows the highest productivity among the Cu-rich materials. It appears that an increase in specific surface area from 104 ($Cu_{64}Zn_{32}Zr_4$) to

117 m^2 g^{-1} ($Cu_{62}Zn_{30}Zr_8$) does not further enhance the catalyst activity. However, increasing the Zr content from 8 to 10 mol% leads to a decrease in productivity without affecting the surface area (117 m^2 g^{-1} for $Cu_{60}Zn_{30}Zr_{10}$), indicating the formation of secondary phases. A further increase in the zirconium content to 16% leads to an increase in productivity. This is most likely due to a further increase in specific surface area (144 m^2 g^{-1} for $Cu_{57}Zn_{27}Zr_{16}$). The positive effect of a larger surface area (over)compensates the negative effect of the formation of secondary phases. Taking this into account, we also compare the surface area specific productivity of the catalysts (Figure 2B): It decreases with an increase in the Zr content supporting the assumption that the improvement in productivity is mostly due to the increase in specific surface area and that excess Zr leads to an increase in less active secondary phases. Here, the preferred interplay between an increase in surface area and the formation of a suitable phase composition can most likely be achieved in the range between 4 and 8 mol% Zr.

The Zn-rich catalyst ($Cu_{35}Zn_{61}Zr_4$) is more active than the Cu-rich catalyst ($Cu_{64}Zn_{32}Zr_4$), regardless of its lower specific surface area. Productivity is increased and maintained over a wider conversion range. This suggests a positive influence of a low Cu:Zn ratio and, as $Cu_{35}Zn_{61}Zr_4$ has a higher aurichalcite fraction (44 vs. 5%), may also indicate beneficial effect of aurichalcite over malachite phases in the catalyst precursor. Generally, the Cu particles in catalyst materials derived from aurichalcite are smaller, but are embedded in bulky aggregates resulting from the mesostructure of aurichalcite. This is undesirable for catalysts for methanol synthesis, but has no negative effect on H14-BP dehydrogenation [43]. Fujita et al. [47] reported that catalysts with a low Cu:Zn ratio are also more active in ethanol dehydrogenation. A high activity of catalysts with a pronounced aurichalcite precursor phase was demonstrated in their study. With the same metal composition, catalysts derived from aurichalcite precursors showed higher conversions than those from malachite precursors attributed to a higher Cu dispersion [47]. This can be seen as an indication that a low Cu:Zn ratio and the associated aurichalcite phases in the catalyst precursor might enhance the performance of the resulting catalyst material in H14-BP partial dehydrogenation.

3.2 | Influence of Catalyst Precursor Synthesis Parameters

The structure of the catalyst precursor is obviously of particular importance for the activity of the corresponding catalyst. In methanol synthesis, Zn malachite is considered to be the precursor resulting in the most active catalysts [48]. This is attributed to the unique microstructure that is formed when Zn malachite is calcined and reduced [14, 43]. Other authors report that catalysts made from aurichalcite precursors show particularly high activity [49, 50]. In aurichalcite, Cu is distributed in the hydroxyl carbonate matrix of Zn [51]. This results in smaller Cu particles and improved Cu dispersion after calcination and reduction [49, 50]. In the ageing step, the crystalline catalyst precursor phases originate from the primary amorphous precipitation products [26]. The final catalyst precursor properties can thereby be influenced by the temperature [52, 53] and the pH of the suspension [15]. Both parameters were specifically varied in this study and their influence on the activity of the resulting catalyst was evaluated.

Firstly, four catalysts with similar compositions but different ageing temperatures are compared. Figure 3 shows the specific surface area and phase composition of the corresponding catalyst precursors.

Catalyst precursors aged at 55 and 60°C consist entirely of malachite. Increasing the ageing temperature leads to the formation of secondary phases as reported in literature [52]. Aurichalcite formation is detected at an ageing temperature of 70°C or higher. Ageing at 80°C increases the proportion of aurichalcite from 25 wt% at 70°C to 37 wt%. An increased aurichalcite content is accompanied by a decrease in the Zn content in the malachite phase. The formation of additional phases also affects the specific surface area of the precatalysts. [52] The pure malachite precatalyst has a specific surface area of 104 m^2 g^{-1}. This value decreases to 97 and 84 m^2 g^{-1} for aging temperatures of 70 and 80°C, respectively, due to the pronounced formation of aurichalcite.

In addition to temperature, pH has a major influence on phase formation during ageing. [15] Zn integration into the malachite structure is facilitated for ageing at an initial pH ≥ 7.0. In contrast, an increase in aurichalcite content at pH 6.5 compared to 7.0 was found [54]. Thus, a lower pH during ageing favors the formation of active secondary phases. In this study two catalysts that were precipitated at a pH of 7.1 and 6.7 are compared. For $Cu_{63}Zn_{30}Zr_7$-6.7, the share of aurichalcite increases from 2 ($Cu_{64}Zn_{32}Zr_4$) to 13 wt%. Despite the use of ZrO_2 as an additive, this is in good agreement with literature for CZA precursor synthesis [54].

Productivity (Figure 4 A) and specific productivity (Figure 4 B) curves for the catalysts whose precursors were aged at different temperatures and different pH values are compared to assess their performance in H14-BP dehydrogenation.

Lowering the initial pH value during ageing induces a clearly observable change in activity of the resulting catalyst ($Cu_{64}Zn_{32}Zr_4$ vs. $Cu_{63}Zn_{30}Zr_7$-6.7). We initially attribute this difference to increased incorporation of Zn into the malachite phase in favor of a relatively increased Cu content in the aurichalcite phase.

Regarding ageing temperature, again a volcano-type behavior can be observed (see also Figure S5). The catalyst derived from the precursor aged at a temperature of 55°C ($Cu_{64}Zn_{32}Zr_4$), which equals the methanol synthesis reference catalyst [26, 27], shows the lowest productivity. Both, 60 and 80°C ageing temperature, led to a slight increase in catalyst productivity, while an ageing temperature of 70°C results in the highest productivity. The reduced specific surface area of $Cu_{62}Zn_{31}Zr_7$-80 (84 m^2 g^{-1}, 18% decrease compared to $Cu_{63}Zn_{32}Zr_5$-60) does not lead to a noticeable change in productivity. According to Figure 3, the aurichalcite content increases as the ageing temperature rises whereas the Zn content of the malachite phase decreases, respectively. In $Cu_{62}Zn_{32}Zr_6$-70 thus a secondary phase becomes detectable (25 wt% aurichalcite) without extensively reducing the Zn content in the malachite phase. For $Cu_{62}Zn_{31}Zr_7$-80, Zn is mainly present in secondary phases and therefore unable to stabilize a high dispersion of Cu. For the dehydrogenation of ethanol to acetaldehyde, it has already

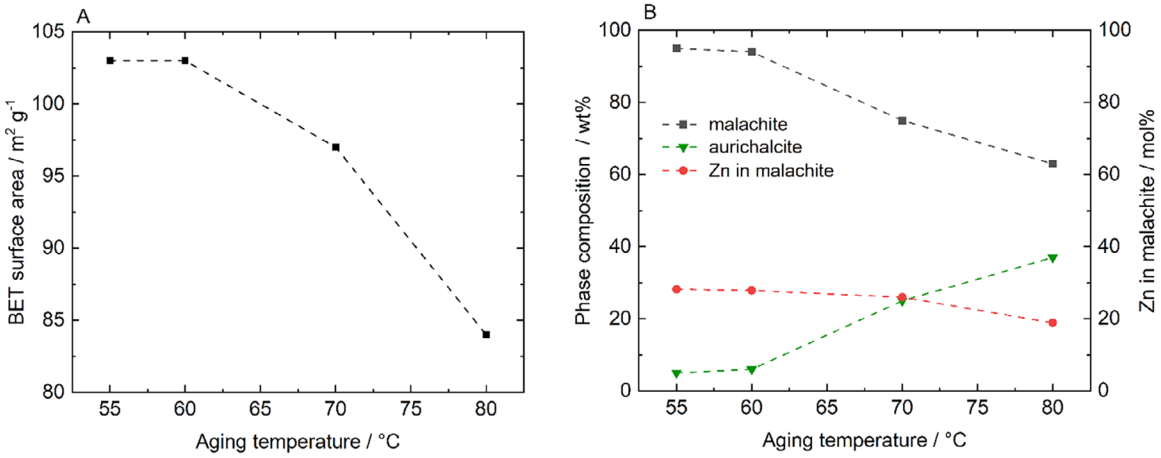

FIGURE 3 | Specific surface area according to the BET-method of precatalysts (A) and composition of the crystal phases (B) plotted against the ageing temperature during the synthesis of the corresponding catalyst precursors.

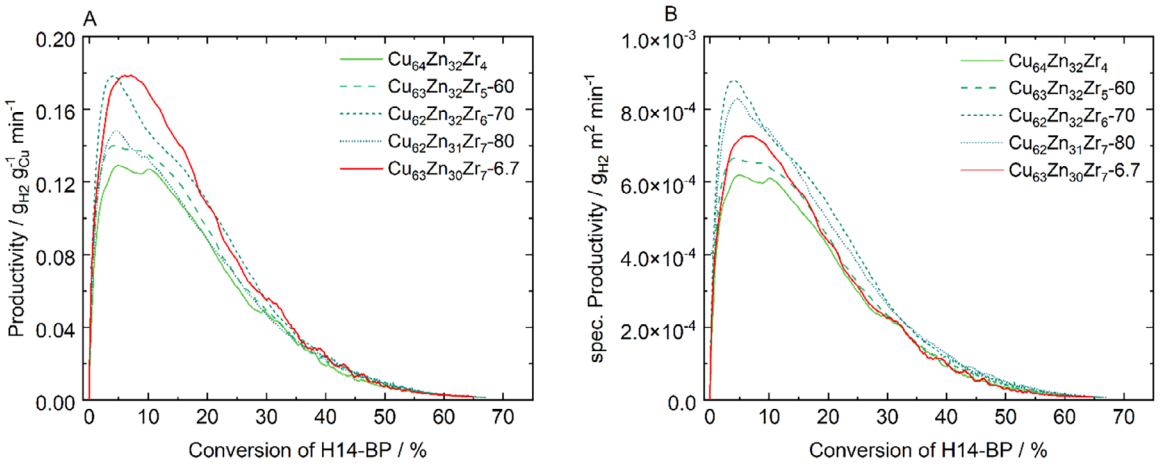

FIGURE 4 | Productivity (A) and specific productivity (B) over conversion of H14-BP of the catalysts aged at different Temperatures and of the catalysts aged at different pH values in the dehydrogenation of H14-BP. Experimental conditions: 170°C; 1 atm; 400 mL min^{-1} Ar; 1 mol% Cu:H14-BP; average from two dehydrogenation experiments.

been shown that aurichalcite contributes to a high catalyst activity, which was attributed to smaller Cu particles present after calcination from aurichalcite precursors [47]. For $Cu_{62}Zn_{31}Zr_7$-80 in contrast, obviously the reduced surface area overcompensates the activity enhancing contribution of the secondary phases: $Cu_{62}Zn_{32}Zr_6$-70 and $Cu_{62}Zn_{31}Zr_7$-80, which both contain aurichalcite, have a similar and significantly higher specific productivity than $Cu_{64}Zn_{32}Zr_4$ and $Cu_{63}Zn_{32}Zr_5$-60, which do not contain significant amounts of secondary phases.

3.3 | Aurichalcite-rich Catalysts

In order to investigate the influence of the aurichalcite content in the catalyst precursor more closely, two further catalyst precursors with high aurichalcite content ($Cu_{60}Zn_{30}Zr_{10}$-80-7.9 with 98 wt% aurichalcite and $Cu_{67}Zn_{33}Zr_0$-70-8.0 with 99 wt% aurichalcite) were synthesized and tested. The most promising precatalyst to this point ($Cu_{62}Zn_{32}Zr_6$-70, see previous section) and one without aurichalcite but a similar metal composition ($Cu_{57}Zn_{27}Zr_{16}$) are selected for comparison. Figure 5 shows the course of productivity (A) and specific productivity (B) plotted against the conversion of H14-BP.

The productivity curve of $Cu_{60}Zn_{30}Zr_{10}$-80-7.9 shows the presumed positive influence of an increased aurichalcite content, which has been achieved by selected precursor synthesis parameters. The increase in the aurichalcite content from 25% ($Cu_{62}Zn_{32}Zr_6$-70) to 98 wt% leads to an increase in maximum productivity of approx. 11% to 0.20 $g_{H2}\ g_{Cu}^{-1}\ min^{-1}$ and, similarly, to increased specific productivity. The slight decrease in specific surface area from 97 to 92 $m^2\ g^{-1}$ has no noticeable effects. For $Cu_{57}Zn_{27}Zr_{16}$ with 0% aurichalcite however, a significant reduction in productivity becomes apparent, with the maximum productivity dropping by 40% to 0.12 $g_{H2}\ g_{Cu}^{-1}\ min^{-1}$.

On the other hand, introducing another aurichalcite-rich catalyst ($Cu_{67}Zn_{33}Zr_0$-70-8.0) shows a strong reduction in productivity. Furthermore, a high deviation between the individual experiments was observed during four reproductions, which was not

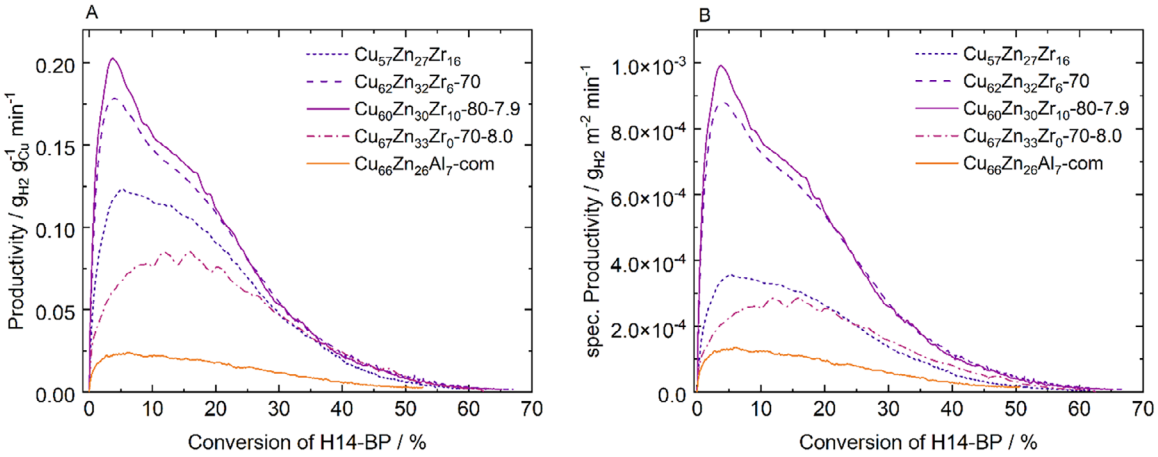

FIGURE 5 | Productivity (A) and specific productivity (B) over conversion of H14-BP of the catalysts with different aurichalcite contents in the dehydrogenation of H14-BP. Experimental conditions: 170°C; 1 atm; 400 mL min^{-1} Ar; 1 mol% Cu:H14-BP; average from two dehydrogenation experiments.

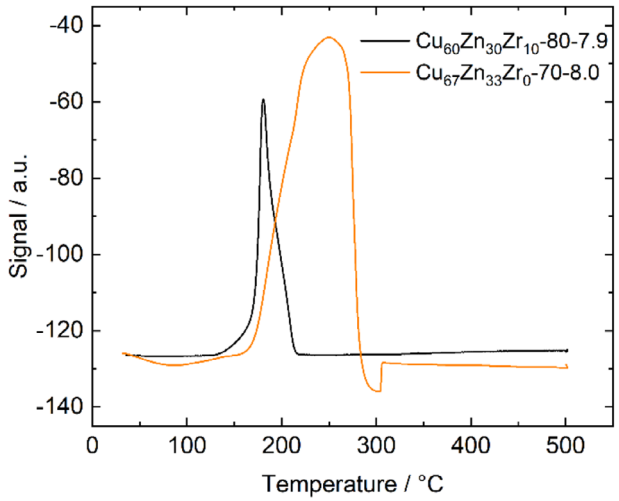

FIGURE 6 | Comparison of the TPR profile of $Cu_{60}Zn_{30}Zr_{10}$-80-7.9 and $Cu_{67}Zn_{33}Zr_0$-70-8.0.

TABLE 3 | Crystallite sizes of $Cu_{60}Zn_{30}Zr_{10}$-80-7.9 and $Cu_{67}Zn_{33}Zr_0$-70-8.0 determined by XRD Rietveld analysis.

Sample	Crystallite size a-axis [nm]	Crystallite size c-axis [nm]
$Cu_{60}Zn_{30}Zr_{10}$-80-7.9	2.6 ± 0.1	4.1 ± 0.1
$Cu_{67}Zn_{33}Zr_0$-70-8.0	9.4 ± 0.3	10.3 ± 0.2

observed for any other catalyst (see Figures S6 and S7). In addition, more variation in reaction onset delay was observed between experiments. This indicates an impairment of the in-situ reduction. To obtain additional clarification on this point, results from TPR measurements and XRD Rietveld analysis of the two materials with similar aurichalcite content ($Cu_{60}Zn_{30}Zr_{10}$-80-7.9 with 98 wt% aurichalcite and $Cu_{67}Zn_{33}Zr_0$-70-8.0 with 99 wt% aurichalcite) are considered (Figure 6 and Table 3).

For $Cu_{67}Zn_{33}Zr_0$-70-8.0 the aurichalcite crystallite size increases. As larger particles are usually less reactive toward reduction, both the temperature of the peak maximum and the onset of reduction increase. Thus, the reaction temperature of 170°C lies in the initial range of the reduction peak of $Cu_{67}Zn_{33}Zr_0$-70-8.0 whereas it almost meets the peak maximum temperature for $Cu_{60}Zn_{30}Zr_{10}$-80-7.9. We speculate that the initial reduction rate at this temperature is slower and the overall reduction might occur less defined for the precatalyst with larger aurichalcite crystallites [55]. Consequently, a similar behavior regarding in-situ reduction during catalytic dehydrogenation with $Cu_{67}Zn_{33}Zr_0$-70-8.0 is a possible explanation of both the low activity and the limited reproducibility in catalytic tests.

3.4 | Summary

From the descriptions above, two main influencing factors on CZZ catalyst productivity in H14-BP partial dehydrogenation were identified: specific surface area of the calcined precatalyst and aurichalcite content in the catalyst precursor. The maximum productivity of all CZZ catalysts under investigation is correlated to their specific surface area after calcination as well as the aurichalcite content in the dried precursor (Figure 7).

It can be derived that activity enhancement from the aurichalcite content in the precursor is more pronounced than from the specific surface area of the precatalyst. The catalyst with the highest productivity is $Cu_{60}Zn_{30}Zr_{10}$-80-7.9 with an aurichalcite content of 98 wt%.

4 | Conclusion

In this work, Cu/ZnO/ZrO_2 (CZZ) catalysts were prepared by continuous co-precipitation followed by suspension ageing. The main goal was to investigate how various factors—such as elemental composition, synthesis temperature, and pH during preparation—affect the catalyst precursor morphology and, ultimately, the catalytic activity in the dehydrogenation of H14-BP as a model reaction.

The results showed that catalysts containing alumina (CZA) had lower productivity compared to those without additive; the

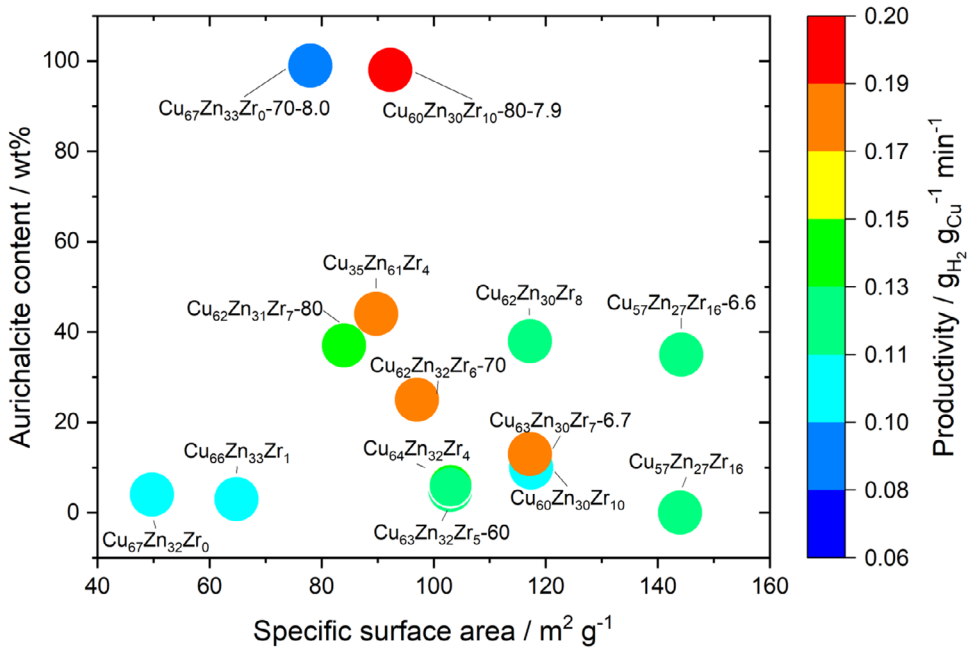

FIGURE 7 | Productivity in H14-BP partial dehydrogenation for all CZZ catalyst materials under investigation depending on specific surface area and aurichalcite content.

highest activity was observed in CZZ catalysts with ZrO_2 as an additive. Regarding the zirconium oxide content, a volcano-type behavior was observed with a maximum in productivity between 4 and 8 mol%. Catalysts with Zn-rich compositions were more active than Cu-rich ones, achieving a maximum productivity of 0.17 $g_{H2}\, g_{Cu}\, min^{-1}$, and maintaining high conversion over a broader range. Structural analyses indicated that the secondary phase aurichalcite, which made up about 44% by weight, positively influenced activity. When ageing temperatures during syntheses ranged from 55 to 80 °C, different phases formed: at 55 and 60 °C only malachite was present, while at 70 °C aurichalcite began to form, and at 80 °C its amount increased further. Interestingly, despite a decrease in specific surface area at higher ageing temperatures, the catalyst aged at 70 °C showed the highest productivity (0.18 $g_{H2}\, g_{Cu}\, min^{-1}$). This suggests that the formation of aurichalcite promotes smaller Cu particles and higher dispersion, which enhances reactivity despite surface area loss. The pH during ageing also plays a role. At initial pH ≥ 7, Zn is less effectively incorporated into malachite, while at lower pH values higher Zn contents through direct phase incorporation are possible. Notably, at an initial pH of 6.7, the content of aurichalcite in the catalyst precursor increased from 2 wt% (at initial pH 7.1) to 13 wt%. The increase in aurichalcite content correlated with a 45% higher maximum productivity, even though the surface area remained similar. To further explore the influence of aurichalcite, additional catalysts with high aurichalcite content (up to 99 wt%) were prepared. The catalyst derived from the 98 wt% aurichalcite precursor showed an 11% higher maximum productivity (0.20 $g_{H2}\, g_{Cu}\, min^{-1}$) compared to the one with 25 wt% aurichalcite, despite having a lower surface area. Another aurichalcite-rich material (99 wt%), in contrast, was associated with low activity and worse reproducibility in catalytic tests, most likely due to a change in reduction behavior because of a larger crystallite size.

Overall, this study demonstrated that CZZ catalysts exhibit higher activity for the dehydrogenation of the alcohol functionality of H14-BP than state-of-the-art CZA and that—unlike in methanol synthesis—aurichalcite secondary phases seem to be related to this. As described, the variation of composition and synthesis procedure are a lever for adjusting beneficial catalyst properties for this model reaction. The findings can be transferred to other similar reactions or serve as basis for advanced material synthesis.

Acknowledgments

This work was funded by the Bavarian Ministry of Economic Affairs, Regional Development and Energy through the project "*Erforschung und Entwicklung eines emissionsfreien und stark emissionsreduzierten Antriebssystems am Beispiel des Schienenverkehrs*". Financial support by the Helmholtz Research Program "Materials and Technologies for the Energy Transition (MTET), Topic 3: Chemical Energy Carriers" is highly acknowledged. Additional support by the Werner Siemens Foundation in the frame of the WSS research center "catalaix: catalysis for a circular economy" is gratefully acknowledged. The authors are grateful for the initiative of Sabrina Polierer in providing profound synthesis concepts.

Open access funding enabled and organized by Projekt DEAL.

Conflicts of Interest

The authors declare no conflict of interest

Data Availability Statement

The data that support the findings of this study are available from the corresponding author upon reasonable request.

References

1. P. Preuster, C. Papp, and P. Wasserscheid, "Liquid Organic Hydrogen Carriers (LOHCs): Toward a Hydrogen-Free Hydrogen Economy,"

Accounts of Chemical Research 50 (2017): 74–85, https://doi.org/10.1021/acs.accounts.6b00474.

2. M. H. Hamayun, I. M. Maafa, M. Hussain, and R. Aslam, "Simulation Study to Investigate the Effects of Operational Conditions on Methylcyclohexane Dehydrogenation for Hydrogen Production," *Energies* 13 (2020): 206, https://doi.org/10.3390/en13010206.

3. M. R. Usman and D. L. Cresswell, "Options for On-Board Use of Hydrogen Based on the Methylcyclohexane–Toluene–Hydrogen System," *International Journal of Green Energy* 10 (2013): 177–189, https://doi.org/10.1080/15435075.2011.647168.

4. N. Brückner, K. Obesser, and A. Bösmann, et al., "Evaluation of Industrially Applied Heat-Transfer Fluids as Liquid Organic Hydrogen Carrier Systems," *Chemsuschem* 7 (2014): 229–235, https://doi.org/10.1002/cssc.201300426.

5. H. Jorschick, S. Dürr, P. Preuster, A. Bösmann, and P. Wasserscheid, "Operational Stability of a LOHC-Based Hot Pressure Swing Reactor for Hydrogen Storage," *Energy Technology* 7 (2019): 146–152, https://doi.org/10.1002/ente.201800499.

6. H. Jorschick, P. Preuster, and S. Dürr, et al., "Hydrogen Storage Using a Hot Pressure Swing Reactor," *Energy & Environmental Science* 10 (2017): 1652–1659, https://doi.org/10.1039/C7EE00476A.

7. T. Rüde, S. Dürr, P. Preuster, M. Wolf, and P. Wasserscheid, "Benzyltoluene/Perhydro Benzyltoluene— Pushing the Performance Limits of Pure Hydrocarbon Liquid Organic Hydrogen Carrier (LOHC) Systems′, Sustain," *Energy & Fuels* 6 (2022): 1541, https://doi.org/10.1039/D1SE01767E.

8. Z. Feng, X. Chen, and X. Bai, "Catalytic Dehydrogenation of Liquid Organic Hydrogen Carrier Dodecahydro-*N*-ethylcarbazole Over Palladium Catalysts Supported on Different Supports," *Environmental Science and Pollution Research* 27 (2020): 36172–36185, https://doi.org/10.1007/s11356-020-09698-w.

9. D. Zakgeym, J. D. Hofmann, L. A. Maurer, et al., "Better Through Oxygen Functionality? The Benzophenone/Dicyclohexylmethanol LOHC-System," *Sustain Energy Fuels* 7 (2023): 1213, https://doi.org/10.1039/D2SE01750D.

10. J. Da Han, Y. S. Jo, and B. S. Shin, et al., "A Novel Eutectic Mixture of Biphenyl and Diphenylmethane as a Potential Liquid Organic Hydrogen Carrier: Catalytic Hydrogenation," *Energy Technology* 7 (2019): 113–121, https://doi.org/10.1002/ente.201700694.

11. A. Beck, M. A. Newton, L. G. A. van de Water, and J. A. van Bokhoven, "The Enigma of Methanol Synthesis by Cu/ZnO/Al2O3-Based Catalysts," *Chemical Reviews* 124 (2024): 4543, https://doi.org/10.1021/acs.chemrev.3c001.

12. S. Fujita, A. M. Satriyo, G. C. Shen, and N. Takezawa, "Mechanism of the Formation of Precursors for the Cu/ZnO Methanol Synthesis Catalysts by a Coprecipitation Method," *Catalysis Letters* 34 (1995): 85–92, https://doi.org/10.1007/BF00808325.

13. B. Bems, M. Schur, A. Dassenoy, H. Junkes, D. Herein, and R. Schlögl, "Relations Between Synthesis and Microstructural Properties of Copper/Zinc Hydroxycarbonates," *Chemistry—A European Journal* 9 (2003): 2039–2052, https://doi.org/10.1002/chem.200204122.

14. M. Behrens, S. Zander, and P. Kurr, et al., "Performance Improvement of Nanocatalysts by Promoter–Iinduced Defects in the Support Material: Methanol Synthesis Over Cu/ZnO:Al," *Journal of the American Chemical Society* 135 (2013): 6061–6068, https://doi.org/10.1021/ja310456f.

15. M. Behrens and R. Schlögl, "How to Prepare a Good Cu/ZnO Catalyst or the Role of Solid State Chemistry for the Synthesis of Nanostructured Catalysts," *Zeitschrift für anorganische und allgemeine Chemie* 639 (2013): 2683–2695, https://doi.org/10.1002/zaac.201300356.

16. E. Lam, K. Larmier, P. Wolf, S. Tada, O. V. Safonova, and C. Copéret, "Isolated Zr Surface Sites on Silica Promote Hydrogenation of CO_2 to CH_3OH in Supported Cu Catalysts," *Journal of the American Chemical Society* 140 (2018): 10530–10535, https://doi.org/10.1021/jacs.8b05595.

17. S. Wild, S. Polierer, T. A. Zevaco, et al., "Direct DME Synthesis on CZZ/H-FER From Variable CO_2/CO Syngas Feeds," *RSC Advances* 11 (2021): 2556, https://doi.org/10.1039/D0RA09754C.

18. S. Tada, A. Katagiri, and K. Kiyota, et al., "Cu Species Incorporated Into Amorphous ZrO_2 With High Activity and Selectivity in CO_2-to-Methanol Hydrogenation," *The Journal of Physical Chemistry C* 122 (2018): 5430–5442, https://doi.org/10.1021/acs.jpcc.7b11284.

19. F. Arena, G. Italiano, and K. Barbera, et al., "Solid-State Interactions, Adsorption Sites and Functionality of Cu-ZnO/ZrO2 Catalysts in the CO2 Hydrogenation to CH3OH," *Applied Catalysis A: General* 350 (2008): 16–23, https://doi.org/10.1016/j.apcata.2008.07.028.

20. K. Larmier, W.-C. Liao, and S. Tada, et al., "CO 2 -to-Methanol Hydrogenation on Zirconia-Supported Copper Nanoparticles: Reaction Intermediates and the Role of the Metal–Support Interface," *Angewandte Chemie International Edition* 56 (2017): 2318–2323, https://doi.org/10.1002/anie.201610166.

21. S. Polierer, J. Jelic, S. Pitter, and F. Studt, "On the Reactivity of the Cu/ZrO 2 System for the Hydrogenation of CO 2 to Methanol: A Density Functional Theory Study," *The Journal of Physical Chemistry C* 123 (2019): 26904–26911, https://doi.org/10.1021/acs.jpcc.9b06500.

22. M. L. Schulte, V. Truttmann, D. E. Doronkin, et al., "Monitoring the Fate of Zn in the Cu/ZnO/ZrO_2 Catalyst during CO_2-to-Methanol Synthesis at High Conversions by Operando Spectroscopy," *Angewandte Chemie (International ed in English)* (2025): e202423281.

23. G. Garbarino, P. Riani, M. Villa García, E. Finocchio, V. Sánchez Escribano, and G. Busca, "A Study of Ethanol Conversion Over Zinc Aluminate Catalyst," *Reaction Kinetics, Mechanisms and Catalysis* 124 (2018): 503–522, https://doi.org/10.1007/s11144-018-1395-z.

24. P. H. Finger, T. A. Osmari, M. S. Costa, J. M. C. Bueno, and J. M. R. Gallo, "The Role of the Interface Between Cu and Metal Oxides in the Ethanol Dehydrogenation," *Applied Catalysis A: General* 589 (2020): 117236, https://doi.org/10.1016/j.apcata.2019.117236.

25. A. G. Sato, D. P. Volanti, D. M. Meira, S. Damyanova, E. Longo, and J. Bueno, "Effect of the ZrO_2 Phase on the Structure and Behavior of Supported Cu Catalysts for Ethanol Conversion," *Journal of Catalysis* 307 (2013): 1–17, https://doi.org/10.1016/j.jcat.2013.06.022.

26. D. Guse, L. Warmuth, M. Herfet, et al., "Seeding as a Decisive Tool for Increasing Space-Time-Yields in the Preparation of High-Quality Cu/ZnO/ZrO_2 Catalysts," *Catal* 14 (2024): 517, https://doi.org/10.3390/catal14080517.

27. L. Warmuth, T. A. Zevaco, and S. Pitter, "In Situ FT-IR Reveals Ageing Phenomena in the Formation of a Cu/Zn/Zr Methanol Catalyst Precursor," *Inorganic Chemistry Communications* 172 (2025): 113753, https://doi.org/10.1016/j.inoche.2024.113753.

28. L. Warmuth, T. A. Zevaco, D. Guse, M. Zimmermann, M. Kind, and S. Pitter, "Phase Transformation Processes in Coprecipitated Cu/Zn/Zr Methanol Catalyst Precursors-Insights Into Suspension Aging Form Ultrafast Nucleation," *ChemPlusChem* 90 (2025): e202500284.

29. M. Behrens, A. Furche, I. Kasatkin, et al., "The Potential of Microstructural Optimization in Metal/Oxide Catalysts: Higher Intrinsic Activity of Copper by Partial Embedding of Copper Nanoparticles," *Chemcatchem* 2 (2010): 816, https://doi.org/10.1002/cctc.201000017.

30. S. Polierer, D. Guse, S. Wild, et al., "Enhanced Direct Dimethyl Ether Synthesis From CO_2-Rich Syngas With Cu/ZnO/ZrO_2 Catalysts Prepared by Continuous Co-Precipitation," *Catal* 10 (2020): 816, https://doi.org/10.3390/catal10080816.

31. N. Doebelin and R. Kleeberg, "Profex: A Graphical User Interface for the Rietveld Refinement Program BGMN," *Journal of Applied Crystallography* 48 (2015): 1573.

32. M. Behrens and F. Girgsdies, "Structural Effects of Cu/Zn Substitution in the Malachite–Rosasite System," *Zeitschrift für anorganische und allgemeine Chemie* 636 (2010): 919–927, https://doi.org/10.1002/zaac.201000028.

33. L. Zwiener, F. Girgsdies, and D. Brennecke, et al., "Evolution of Zincian Malachite Synthesis by Low Temperature Co-Precipitation and Its Catalytic Impact on the Methanol Synthesis," *Applied Catalysis B: Environmental* 249 (2019): 218–226, https://doi.org/10.1016/j.apcatb.2019.02.023.

34. M. Thommes, K. Kaneko, and A. V. Neimark, et al., "Physisorption of Gases, With Special Reference to the Evaluation of Surface Area and Pore Size Distribution (IUPAC Technical Report)," *Pure and Applied Chemistry* 87 (2015): 1051–1069, https://doi.org/10.1515/pac-2014-1117.

35. S. Brunauer, P. H. Emmett, and E. Teller, "Adsorption of Gases in Multimolecular Layers," *Journal of the American Chemical Society* 60 (1938): 309–319, https://doi.org/10.1021/ja01269a023.

36. L. A. Maurer, C. V. Pham, and B. Fritsch, et al., "Improving Hydrogen Release From Oxygen-Functionalized LOHC Molecules by Ru Addition to Pt/C Catalysts," *Chemcatchem* 16 (2024): e202400375, https://doi.org/10.1002/cctc.202400375.

37. D. Strauch, P. Weiner, and B. B. Sarma, et al., "Bimetallic Platinum Rhenium Catalyst for Efficient Low Temperature Dehydrogenation of Perhydro Benzyltoluene," *Catalysis Science & Technology* 14 (2024): 1775–1790, https://doi.org/10.1039/D3CY01336G.

38. F. Pepe and R. Polini, "Catalytic Behavior and Surface Chemistry of Copper/ZnO/Al2O3 Catalysts for the Decomposition of 2-Propanol," *Journal of Catalysis* 136 (1992): 86–95, https://doi.org/10.1016/0021-9517(92)90108-T.

39. D. Guse, S. Polierer, S. Wild, S. Pitter, and M. Kind, "Improved Preparation of Cu/Zn-Based Catalysts by Well-Defined Conditions of Co-Precipitation and Aging," *Chemie Ingenieur Technik* 94 (2022): 314–327, https://doi.org/10.1002/cite.202100197.

40. N. Mota, R. Guil-Lopez, B. G. Pawelec, J. L. G. Fierro, and R. M. Navarro, "Highly Active Cu/ZnO–Al Catalyst for Methanol Synthesis: Effect of Aging on its Structure and Activity," *RSC Advances* 8 (2018): 20619–20629, https://doi.org/10.1039/C8RA03291B.

41. B. Mockenhaupt, J. K. Wied, and S. Mangelsen, et al., "Phase Evolution, Speciation and Solubility Limit of Aluminium Doping in Zinc Oxide Catalyst Supports Synthesized Via Co-Precipitated Hydrozincite Precursors," *Dalton Transactions* 52 (2023): 5321–5335, https://doi.org/10.1039/D3DT00253E.

42. M. Behrens, F. Studt, I. Kasatkin, et al., "The Active Site of Methanol Synthesis Over Cu/ZnO/Al_2O_3 Industrial Catalysts," *Science* 336 (2012): 893, https://doi/10.1126/science.1219831.

43. M. Behrens, "Meso- and Nano-Structuring of Industrial Cu/ZnO/(Al_2O_3) Catalysts," *Journal of Catalysis* 267 (2009): 24–29, https://doi.org/10.1016/j.jcat.2009.07.009.

44. Y. H. Wang, W. G. Gao, Y. E. Zheng, and H. Wang, "The Influence of Zn/Zr Ratios on CuO-ZnO-ZrO_2 Catalysts for Methanol Synthesis From CO_2 Hydrogenation′," *Advances in Materials Research* 941–944 (2014): 425.

45. V. L'hospital, L. Angelo, Y. Zimmermann, K. Parkhomenko, and A.-C. Roger, "Influence of the Zn/Zr ratio in the Support of a Copper-Based Catalyst for the Synthesis of Methanol From CO2," *Catalysis Today* 369 (2021): 95–104, https://doi.org/10.1016/j.cattod.2020.05.018.

46. S. Speakman, "Introduction to X-Ray Powder Diffraction Analysis", (accessed on May 25, 2023), http://prism.mit.edu/xray/introduction%20to%20xrpd%20data%20analysis.pdf .

47. S. Fujita, N. Iwasa, H. Tani, W. Nomura, M. Arai, and N. Takezawa, "Dehydrogenation of Ethanol over Cu/ZnO Catalysts Prepared From Various Coprecipitated Precursors," *Reaction Kinetics and Catalysis Letters* 73 (2001): 367–372, https://doi.org/10.1023/A:1014192214324.

48. J. Zhong, X. Yang, Z. Wu, B. Liang, Y. Huang, and T. Zhang, "State of the Art and Perspectives in Heterogeneous Catalysis of CO_2 Hydrogenation to Methanol", *Chemical Society Reviews* 2020, 49, 1385.

49. T. Fujitani and J. Nakamura, "The Effect of ZnO in Methanol Synthesis Catalysts on Cu Dispersion and the Specific Activity," *Catalysis Letters* 56 (1998): 119–124, https://doi.org/10.1023/A:1019000927366.

50. T. Fujitani and J. Nakamura, "The Chemical Modification Seen in the Cu/ZnO Methanol Synthesis Catalysts," *Applied Catalysis A: General* 191 (2000): 111–129, https://doi.org/10.1016/S0926-860X(99)00313-0.

51. V. Pospelova, J. Aubrecht, K. Pacultová, M. Lhotka, O. Kikhtyanin, and D. Kubička, "Does the Structure of CuZn Hydroxycarbonate Precursors Affect the Intrinsic Hydrogenolysis Activity of CuZn Catalysts?," *Catalysis Science & Technology* 10 (2020): 3303–3314, https://doi.org/10.1039/D0CY00143K.

52. E. Frei, A. Schaadt, T. Ludwig, H. Hillebrecht, and I. Krossing, "The Influence of the Precipitation/Ageing Temperature on a Cu/ZnO/ZrO 2 Catalyst for Methanol Synthesis From H 2 and CO 2 Temperature on a Cu/ZnO/ZrO_2 Catalyst for Methanol Synthesis From H_2 and CO_2," *Chemcatchem* 6 (2014): 1721–1730, https://doi.org/10.1002/cctc.201300665.

53. R. Raudaskoski, M. V. Niemelä, and R. L. Keiski, "The Effect of Ageing Time on Co-Precipitated Cu/ZnO/ZrO_2 Catalysts Used in Methanol Synthesis From CO_2 and H_2," *Topics in Catalysis* 45 (2007): 57–60, https://doi.org/10.1007/s11244-007-0240-9.

54. S. Zander, B. Seidlhofer, and M. Behrens, "In Situ EDXRD Study of the Chemistry of Aging of Co-Precipitated Mixed Cu,Zn Hydroxycarbonates-Consequences for the Preparation of Cu/ZnO Catalysts," *Dalton Transactions* 2012, 41, 13413.

55. Micromeritics, "Application Note 120, Temperature-Programmed Reduction Using the AutoChem", (accessed on November 5, 2025), https://micromeritics.com/resources/temperature-programmed-reduction-using-the-autochem/.

Supporting Information

Additional supporting information can be found online in the Supporting Information section.

Supporting File 1: cctc70570-sup-0001-SuppMat.docx.